A quantitative study of cotyledon positioning in conifer development

David M. Holloway[1,3], Byron Brook[2], JooHyun Kang[2], Cameron Wong[2], Michael Wu[2]

[1]Mathematics Department and [2]Biotechnology Program

British Columbia Institute of Technology

Burnaby, B.C., V5G 3H2, Canada

[3]Biology Department

University of Victoria,

Victoria, B.C.

[1] Corresponding author

David_Holloway@bcit.ca

Tel: 604-456-8199

Fax: 604-432-9173

Abstract

The number of cotyledons in angiosperm monocots and dicots is tightly constrained. But in the gymnosperm Pinaceae, including conifers, cotyledon number (n_c) can vary widely, commonly between 2 to 12. Conifer cotyledons form in whorled rings, on a domed embryo geometry. We measured embryo diameters and counted cotyledons to determine the radial positioning of the whorl and the circumferential spacing between cotyledons. Results were similar between Douglas fir (*Pseudotsuga*), Sitka spruce (*Picea*) and larch (*Larix*), indicating a common mechanism for cotyledon positioning in conifers. Disrupting transport of the growth regulator auxin (with NPA) led to cup-shaped embryos, indicating that whorl (ring) formation is separable from cotyledon patterning within the ring. NPA inhibits cotyledon outgrowth, but not the spacing (distance) between cotyledons. The NPA effect is direct; it does not operate indirectly on embryo size. These results support a hierarchical model for cotyledon positioning in conifers, in which a first stage (not requiring auxin transport) sets the whorl position, constraining the second stage (which requires auxin transport) to form cotyledons within this whorl. Similarly, recent studies in *Arabidopsis* have shown that different components of complex developmental patterns can have different transport properties; this aspect of patterning may be shared across plants.

Key words: cotyledon; somatic embryo; conifer; morphogenesis; polar auxin transport; pattern formation

Introduction

As the first lateral organs, cotyledons offer a unique window into very early stages of signalling, spatial patterning and differentiation in plant development. Unlike angiosperm monocots or dicots, the gymnosperm family of Pinaceae, including conifers, can have highly variable numbers of cotyledons. This polycotyledony has been well known for over a century - based on their own and previous work, Butts and Buchholz (1940) summarized averages and ranges for cotyledon number (n_c) in seed embryos for nearly 200 conifer species. This indicated that mean cotyledon number varies between species from, for example, $\bar{n}_c$ = 3 (*Tsuga*, hemlock) to $\bar{n}_c$ = 9 (*Cedrus*, cedar). n_c variation within species was also found to be large, with standard deviation/mean (CV) typically around 12% (ibid.). Fig. 1*ab* shows an example of such n_c variability within a clonal line of larch (*Larix*). The variability in Pinaceae provides an avenue for studying number selection and organ positioning free of the rigid n_c canalization seen in monocots and dicots. In this way, conifer cotyledon formation can provide insight into fundamental developmental questions, in particular how genetic, biochemical and physical mechanisms control the spatial patterning of organs.

Studying development in conifer seeds presents a number of difficulties (e.g. dissecting and observing an embryo from a seed). Observation and experimental manipulation of conifer embryos is greatly improved in somatic cultures (Attree and Fowke 1993), with naked embryos and suspensor cells maintained on media. In addition, use of clonal lines for somatic cultures controls for genetic variability, allowing for the direct investigation of environmental, physical and chemical effects on development. In somatic larch (*Larix*) cultures, von Aderkas (2002) reported a lower mean and higher variability for n_c than in zygotic (seed) embryos. He also demonstrated that $\bar{n}_c$ is not genetically determined for a species (or culture line), by lowering $\bar{n}_c$ with application of the plant growth regulator (PGR) benzyladenine (BA). Somatic embryos in larch (Harrison and von Aderkas 2004) are largely within the range of 4 – 8 n_c

reported for zygotic embryos (Butts and Buchholz 1940), but the higher somatic standard deviation (s_c = 1.6, vs. s_c = 0.8 zygotic) indicates their distribution is less sharply peaked than the zygotic distribution.

Conifer polycotyledony involves more complex, higher dimensional, spatial patterning than does monocot or dicot development. For dicots, 2 cotyledons can define a line on a tissue. 3 organs can also be positioned in a line, or they can define a higher dimension with a triangular arrangement. Patterns of 3 or more organs can also range from regular to random, and be either evenly distributed over a tissue or constrained to particular sectors. In the case of the early dome-shaped conifer embryo (Fig. 1*c*), cotyledons could be placed (randomly or regularly) all over the surface of the dome, or they could be limited to particular sub-regions. Conifer cotyledons always form in a whorl (or ring), indicating that while the number of cotyledons is highly variable, the restriction of patterning to a sub-region of the embryo is highly conserved. With this restriction of the whorl to a particular 'latitude' of the embryo dome (or particular distance from the embryo centre or outer edge, see Fig. 1*e* red), cotyledon positioning can be regarded in terms of two 1D patterning components operating in orthogonal dimensions. The first patterning component, **P1**, controls the ring position along the radial coordinate *r* (Fig. 1*e*, red band), while the second component, **P2**, controls the positioning of cotyledons within this ring, along the circumferential coordinate ϕ, (Fig. 1*ef*, black dots). The observed regular inter-cotyledon spacing λ (Figs. 1*abef*, double-headed arrows) is associated with the **P2** component. With the relatively short-scale λ, cotyledons could be fit all over the embryo surface if there were no radial constraint from **P1** (especially for larger embryos). Tissue growth proportional to the **P1** ring pattern could produce the early dome flattening observed in normal somatic development (Fig. 1*c* to 1*d*), as well as a later cup-shaped morphogenesis observed in abnormal development. Growth proportional to the **P2** pattern would produce the distinct, separated cotyledons of normal development. Quantitative data in this paper sheds new light on the **P1** and **P2** aspects of patterning, which in turn constrains the potential physical or chemical mechanisms which could control cotyledon positioning in conifers.

A number of physical and chemical mechanisms have been characterized for spatial patterning in development. Physically, the mechanical properties of plant cells and tissues can produce characteristic types of shape change (e.g. Hamant et al. 2008; Rojas et al. 2011; Kroeger et al. 2011; Bassel et al. 2014), as well as produce buckling patterns with characteristic spacing (or wavelength; e.g. Martynov 1975). Chemically, reaction-diffusion mechanisms (Turing 1952) have been extensively explored for plant development, in which activation-inhibition kinetics between two or more chemicals, coupled with diffusion, produce regularly spaced concentration waves with a characteristic wavelength (e.g. Harrison et al. 1981; Lacalli 1981; Meinhardt 1984; Jönsson et al. 2005; Holloway and Harrison 1999, 2008; Digiuni et al. 2008). Such concentration waves have been proposed for the spatial patterning of growth catalysts underlying morphogenesis (e.g. involved in localized relaxation of walls, or localized synthesis of wall material). More recently, the detailed molecular biology of the transport of the PGR auxin has been combined with computational modelling to characterize the unique dynamics of auxin patterning (e.g. Mitchison 1981; Smith et al. 2006; de Reuille et al. 2006; Jönsson et al. 2006). Auxin can polarize its own flow (polar auxin transport, PAT), and the combination of passive (diffusional) and active ('up-the-gradient') auxin transport can produce regular concentration patterns which can control morphogenesis.

Combined experimental and modelling work in the dicot *Arabidopsis* in recent years has shown the role of PAT in numerous developmental systems, including embryos (Friml 2003), roots (Laskowski et al. 2008), leaves (Bilsborough et al. 2011) and flowers (van Mourik et al. 2012). Homologs for a number of the molecules involved in *Arabidopsis* PAT have been found in recent years in conifer embryos (spruce, *Picea abies*; Larsson et al. 2008, 2012*a*, 2012*b*; Hakman et al. 2009; Palovaraa et al. 2010*a*, 2010*b*). These indicate that PAT patterning could be present in conifer development, with similar molecular components to *Arabidopsis*. The most direct experiments on PAT in conifers have been to culture somatic spruce embryos with NPA (1-N-naphthylphthalamic acid), an inhibitor of auxin transport

(Larsson et al. 2008; Hakman et al. 2009). This decreased cotyledon formation and increased aberrant embryo forms, showing that auxin does play a role in conifer cotyledon morphogenesis. However (as discussed above), patterning for n_c > 2 conifers is intrinsically more complex than what has been studied to date for n_c = 2 *Arabidopsis*; in this paper, we present new NPA experimental data bearing specifically on the **P1** and **P2** aspects of conifer cotyledon patterning.

Harrison and von Aderkas (2004) provided the first explanation for conifer n_c variability: they found a clear linear trend between n_c and embryo diameter in larch, indicating that n_c variability is at least in part due to size variability. I.e., the larger the embryo, the more cotyledons it will tend to have. Given that conifer cotyledons form in a circular whorl, the linear relation between embryo diameter, *d*, and n_c can be expressed as:

(1) $$d = (\lambda/\pi)n_c + b$$

where the slope is the distance between cotyledons within the circular whorl λ (Fig. 1*abef*; **P2** spacing along the ϕ coordinate), divided by π; and half of the y-intercept *b* is the distance of the whorl from the edge of the embryonic tissue (Fig. 1*ef*; **P1** spacing along the *r* coordinate). (*d*-*b*) is the diameter of the whorl. Since **P1** and **P2** patterning may be operating before the physical appearance of cotyledons, it is critical to measure embryo diameter at the very first manifestation of the cotyledons (Fig. 1*d*): diameter continues to increase after this point, while n_c is generally stable (this early fixing of organ number was also observed in algal whorl formation; Dumais and Harrison 2000). From linear regression and Eq. 1, Harrison and von Aderkas (ibid.) found λ = 98 μm for larch. They also showed (ibid.) that BA reduction of n_c (as observed in von Aderkas 2002) does not involve a direct effect on this circumferential **P2** patterning: BA treatment does not directly change λ (the slope of Eq. 1), rather it indirectly reduces n_c by reducing embryo diameter. The inter-cotyledon spacing λ implies a mechanism with the capacity to form periodic **P2** patterns.

Periodic patterns are characterized in terms of harmonic modes. For example, patterning (vibration) of a 1D violin string is quantified in terms of sinusoidal modes (each characterized by amplitude and wavelength parameters); on a 2D circular disk, harmonics are Bessel polynomials (e.g. drum-head displacement modes); and on a domed 2D surface (in 3D space), they are the surface spherical harmonics (a set of polynomials; e.g. displacement modes for a domed bell). Chemical and mechanical theories of periodic biological pattern formation have these same harmonic solutions (e.g. diffusion, a transport mechanism in many chemical patterning theories, can produce concentration waves with these harmonics).

The constant inset *b* in Eq. 1 implies that as n_c and diameter increase, the non-cotyledon smooth region interior to the whorl should also increase. This is observed, and Harrison and von Aderkas (2004) discussed how the diameter-dependence of both radial (*r*) and circumferential (ϕ) positioning would be a natural consequence of Bessel disk harmonics (considering the top of the flattened-dome stage embryo, Fig. 1*d*). To more precisely characterize the patterning modes available on the embryo geometry, Nagata et al. (2013) analyzed the harmonics for a reaction-diffusion mechanism on a flattening dome, specified by a parameter γ (Fig. 1*e*) varying between 1 (hemispherical dome) and 0 (flat disk). This quantified the dependence of pattern selection on the 3D embryo geometry, in particular the ranges of diameter and flatness associated with each n_c.

In the current work, we present new quantitative measurements of cotyledon formation in Douglas fir and spruce. This indicates that the linear correlation between diameter and n_c is general to conifers. The regression parameters from this data indicate (in concert with the analytical results above) that cotyledons are not patterned on the flattened-top stage (Fig. 1*d*), but at some time prior to this (i.e. between Figs. 1*c* and 1*d*). NPA treatment shows that ring formation (**P1**) and cotyledon outgrowth (**P2**) are separable: NPA interference with PAT shuts off cotyledon formation and results in cup-shaped embryos. Through diameter measurements, we show that this is a direct effect on the patterning of

cotyledon position, and not an indirect effect via embryo size. NPA is therefore the first substance shown to directly affect cotyledon morphogenesis in conifers. These results support a 2-stage hierarchical mechanism for cotyledon positioning, with **P1** (not requiring PAT) setting the radial whorl position which constrains where **P2** (requiring PAT) forms cotyledons. By cutting off **P2** patterning with NPA we can directly observe the **P1** ring patterning which, in normal development, underlies the reduction in dimensionality constraining cotyledons to form in a quasi-1D whorl rather than over the whole 2D surface of the embryo.

Recent studies in *Arabidopsis* have shown similar cases, in which different aspects of a complex patterning process can differ in their PAT dependence or use different types of PAT. Larsson et al. (2014) treated developing flowers with NPA, and found that increased exposure produced increasingly strong effects on lateral structures of the gynoecium while leaving medial structures relatively unaffected. Similar to the conifer cotyledon results reported here, this suggests two components of gynoecial development: PAT-independent medial differentiation; and PAT-dependent lateral differentiation. Even within PAT-dependent morphogenesis, different pathways can be involved in different aspects of patterning: Furutani et al. (2014) were able to distinguish two types of PAT in the shoot apex, finding that in *MAB4* mutants, surface flux was retained, but basipetal (inward) flow was lost, disrupting growth of organ primordia. While it is hoped that molecular approaches with such sophisticated genetic manipulation and imaging tools will become increasingly available in conifers, the present study uses an alternate quantitative approach and the phenomenon of conifer polycotyledony to show that differential regulation of flow can underlie complex morphogenesis in non-model plants.

Materials and methods

Cultures: Somatic embryo cultures of Douglas fir (*Pseudotsuga menziesii*) and Sitka spruce (*Picea sitchensis*) were obtained from the von Aderkas lab at the University of Victoria. Measurements were

made on one fir clonal line, DF-G, and two spruce lines, SK and 2L13. Cultures were transferred to new media every week and grown in the dark.

Maintenance: Cultures were maintained in sterilized phytagel-based Litvay medium, modified by increasing $CaCl_2$ 20-fold and not adding NH_4NO_3. For Douglas fir, to this was added 10g/L glucose, 10 µM 2,4-D (2,4-dichlorophenoxyacetic acid), 5 µM BA (benzyladenine), and 0.2 g/L each of glutamine and casein hydrolysate. For spruce, sucrose was used instead of glucose, and concentrations were adjusted to 20 µM 2,4-D, 10 µM BA, 0.4 g/L glutamine and 0.8 g/L casein hydrolysate. pH was adjusted to 5.8.

Maturation: Embryo development was induced by transfer to maturation media of modified Litvay's, plus, for Douglas fir, 30g/L maltose, 10g/L galactose, 100 g/L PEG1500, 10 g/L lactose, 60 µM ABA (abscisic acid), 0.2 g/L glutamine, and 0.2 g/L casein hydrolysate. For spruce, the only sugar was sucrose, 30 g/L, plus 0.2 g/L NH_4NO_3, 0.4 g/L glutamine, and 0.8 g/L casein hydrolysate. pH was adjusted to 5.8.

NPA treatment: a 1 mM stock solution of NPA (1-N-naphthylphthalamic acid; OlChemIM, Czech Republic) was made in DMSO (dimethyl sulfoxide), as in Hakman et al. (2009), and added to maturation media to make final concentrations of 0.02, 0.04, 0.06, 0.08, 0.1, 0.4, 0.7 and 1.0 µM in the culture dishes. In NPA-treatment experiments, cultures were transferred from maintenance media to NPA-containing maturation media; i.e. embryo development was entirely NPA-exposed in these cases (as in Hakman et al. 2009).

Temperature: cultures were kept in a growth chamber at 20˚C. For raised temperature experiments, small growth chambers at 24˚C and 30˚C were used.

Classification: Just after the flattened top stage (Fig. 1*d*), we found that most embryos could be classified as either CoN (clearly countable, regularly spaced cotyledons; Fig. 2*a*) or AnCR (annular cup forming, with no cotyledons; Fig. 2*b*). (See Harrison and von Aderkas (2004) for naming conventions.) Classification at later stages (e.g. Hakman et al. 2009) incorporates later morphological events, such as

cotyledon fusions, which do not reflect the initial **P1**, **P2** patterning. We classified a small proportion of the early embryos as cotyledon-like, but deformed (CoN-Def) or cup-like, but deformed (AnCR-Def). These included fusions (e.g., an outgrowth twice the width of a normal cotyledon initial); split cups (e.g. where a smooth cup ridge had one or more divisions); partial cup ridges mixed with some distinct cotyledons; a single bump inside the whorl (perhaps an early appearance of the shoot apical meristem); some cotyledons inset from the main whorl; and gaps, where a cotyledon whorl was missing one or more members (Fig. 2*c*).

Measurements: Cultures were grown either in embryonal suspensor masses or separated out onto gridded filter paper (for easier tracking of individual embryos). We measured no morphogenetic differences between the techniques. After transfer to maturation media, tissues were monitored once a week until domed embryos appeared (roughly 4 weeks). At this point, individual embryos were tracked and observed every few days during dome flattening, until a diameter measurement and cotyledon count could be made at the first appearance of cotyledon initials (CoN embryos). A follow-up measurement was made approximately one week after this, to confirm n_c. Linear correlation and regression were calculated on diameter and n_c data from CoN embryos, to determine the λ and b parameters in Eq. 1. Diameter measurements were made similarly for cup-shaped embryos (AnCR), at the flat-topped stage, when a distinct ridge was just becoming visible. Observations were through a Nikon SMZ-2T dissecting microscope, with an eyepiece micrometer for measuring diameter. Two external lights on flexible arms were adjusted to maximize contrast during observations.

Results

Distribution of cotyledon number in spruce and Douglas fir

To test whether the distribution of n_c found by Harrison and von Aderkas (2004) is larch-specific or is more general in conifer species, we measured n_c in large samples of somatic embryos of spruce

(*Picea sitchensis*; *N* = 326) and Douglas fir (*Pseudotsuga menziesii*; *N* = 127). Similar to larch (ibid.), we see that n_c peaks around 4 – 6 for both spruce and fir (Fig. 3), suggesting a common n_c distribution profile across conifers. Our data indicate that spruce has a higher mean n_c than larch (t-test, $p < 0.01$; $\bar{n}_c$ = 5.8 for spruce in our data; $\bar{n}_c$ = 5.0 in the larch data, ibid.), in agreement with observations in seed embryos (Butts and Buchholz 1940). Our data also indicate that spruce has a larger mean n_c than Douglas fir ($\bar{n}_c$ = 5.3; t-test, $p < 0.01$). (Results unaffected by removal of the two spruce embryos at n_c 12 and 13.) The standard deviations for both spruce and Douglas fir are comparable to that seen for larch (Harrison and von Aderkas 2004), indicating a similar breadth of the n_c distribution across conifers for somatic embryos.

A characteristic cotyledon spacing across conifers

We find significant linear correlation ($p < 0.01$ that $\rho = 0$) between embryo diameter and n_c in spruce and Douglas fir (Fig. 4), suggesting that the diameter dependence of n_c-variation is general across conifers. For Douglas fir, the slope of the n_c-diameter regression (Fig. 4) converts (via Eq. 1) to an inter-cotyledon spacing in the whorl of λ = 110 µm (95% CI [73, 150]). For the spruce data, the two highest n_c embryos (n_c 12 and 13) appear off-trend of the other 324 embryos measured. Without these outliers, the value of the spruce inter-cotyledon spacing λ is also 110 µm (95% CI [87, 130]); with the outliers, λ is calculated at 97 µm (c.f. 98 µm for larch in Harrison and von Aderkas 2004).

Effect of temperature

Due to the temperature dependence of tissue mechanical properties, chemical reaction rates and transport properties, a physical or chemical mechanism controlling cotyledon spacing might be expected to alter λ in response to a temperature shift (see Harrison et al. 1981, for temperature shift experiments on algae morphogenesis). We matured spruce cultures at two elevated temperatures

(compared to the 20˚C growth chamber): 24˚C and 30˚C. Significant linear correlation was found for diameter vs. n_c measurements in these experiments: at T = 20˚C, N = 25, r = 0.70, $p < 0.01$ that ρ = 0; at T = 24˚C, N = 28, r = 0.39, $p < 0.05$ that ρ = 0; at T = 30˚C, N = 28, r = 0.82, $p < 0.01$ that ρ = 0. There was no significant difference between any of the regression slopes at the three temperatures ($p > 0.8$, pairwise t-tests, $t = \frac{b_{1A} - b_{1B}}{\sqrt{S_{eA}^2 + S_{eB}^2}}$, for slopes b_1 from two populations A and B, with S_e standard error of the regression), indicating that the developmental process controlling cotyledon spacing λ is buffered within this temperature range.

NPA treatment affects cotyledon formation

Larsson et al. (2008) first reported an effect of NPA treatment on conifer embryos, showing that polar auxin transport was necessary for normal development. Hakman et al. (2009) subsequently treated cultures with increasing concentrations of NPA. They found the percentage of normal cotyledon development compared to 'other' development (their classification for poorly separated cotyledons, one cotyledon, or no cotyledons) decreased with NPA concentration: from 70% normal at 0 µM NPA (out of 60 embryos); to 30% normal at 0.1 µM NPA (out of 80 embryos); to 0% normal at 1 µM NPA (out of 60 embryos). To understand the effects of NPA on cotyledon formation more quantitatively, we measured diameters and counted cotyledons at their first appearance (see Methods), several weeks earlier than the advanced cotyledon stages reported in Larsson et al. (2008) and Hakman et al. (2009). In addition, we ran experiments at a series of intermediate NPA concentrations, to more closely investigate the morphological transition between 0 and 1 µM.

<u>Increasing NPA increases prevalence of cup-shaped embryos</u>

Table 1 shows the CoN:AnCR ratio (regularly-spaced cotyledons vs. cup-shaped embryos) for several different experiments across a range of NPA concentrations. (The trends in Table 1 are unaffected by leaving out CoN-Def and AnCR-Def embryos.) The propensity for forming CoN embryos varies across culture lines and between different experiments of the same line, even in the absence of NPA: the SK line was very favourable for CoN development, while the 2L13 line showed similar CoN percentages to Hakman et al. (2009) in some experiments, and lower percentages in others. Nevertheless, all experiments showed a clear drop in CoN formation with increasing NPA concentration. As in Hakman et al. (2009), we see the CoN:AnCR ratio dropping between 0 to 0.1 µM NPA (top row, SK), but with a larger effect than in their lines. Hakman et al. observed no cotyledons at 1.0 µM NPA; with a larger sample size, we observed several embryos forming cotyledons at this concentration. The CoN:AnCR ratio for 0.4, 0.7 and 1.0 µM NPA are all similar to each other and about $1/10^{th}$ the CoN:AnCR ratio at 0.1 µM NPA, indicating a distinct shift to AnCR morphogenesis above a threshold NPA concentration. Finer scale concentration divisions show that this threshold is above 0.06 µM NPA in CoN-favourable cultures; while the threshold may be lower, around 0.02 to 0.04 µM NPA, in cultures which are less favourable to cotyledon formation.

Diameter is not responsible

We next checked whether the CoN to AnCR change in morphology was due to a change in size, as is the case with BA treatment, where reduction of n_c (von Aderkas 2002) is due to a reduction of diameter (Harrison and von Aderkas 2004). For NPA, the induced morphological change is *not* due to a change in diameter: Fig. 5 shows histograms of AnCR and CoN embryos by diameter for the 2L13 embryos from Table 1. Mean diameters are equal for both AnCR and CoN embryos without NPA (Fig. 5*a*); and are still equal for AnCR and CoN embryos with 0.08 µM NPA treatment, despite a large drop in the proportion of CoN embryos at this concentration (Fig. 5*b*). This holds for all low concentration NPA

treatments (2L13 line), with no difference in CoN and AnCR diameters (Fig. 5*c*). At higher NPA treatment, we begin to see smaller AnCR embryos, on average, than CoN (Fig. 5*d*, SK line). However, there is a large overlap in diameters at any NPA concentration, indicating that diameter change is not responsible for the morphological transition from CoN to AnCR with increasing NPA concentration.

Inter-cotyledon spacing λ is unaffected by NPA; CoN formation at low NPA

There is significant linear correlation ($p < 0.05$) between n_c and diameter at all NPA levels where CoN is predominant (Table 1: 0 (SK and 2L13 experiment 1), 0.02, 0.04 and 0.06 μM NPA (2L13 experiment 1)). The slopes from these regressions (λ/π) are statistically indistinguishable from one another ($p > 0.8$ in pairwise t-tests; null hypothesis of no difference), and from the slopes for fir (Fig. 4b) and larch (Harrison and von Aderkas 2004). This supports that there is a characteristic λ for conifers, and that it is not affected by NPA at levels where inter-cotyledon spacing can be calculated from Eq. 1 (i.e. where CoN formation is robust enough for linear regression).

Intermediate to high NPA

Higher NPA concentration treatments show the qualitative shift from CoN to AnCR morphology (Table 1). At high NPA (1.0 μM) all AnCR embryo 'cups' had smooth rims, while at intermediate NPA (0.1 to 0.7 μM) we observed some AnCR embryos with 'rough-ridges' (in which small bumps formed on the rims of the cups). CoN embryos are rare in these conditions (and insufficient for calculating λ via Eq. 1). The CoN embryos which do form, however, fall on the n_c vs. diameter scatterplot for the 0 NPA control embryos (Fig. 6). The NPA treated embryos tend to be larger than the control for a given n_c. That is, they are consistent with the 0 NPA slope (supporting the non-difference in slopes at low NPA, previous sub-section), but tend to be above the 0 NPA regression line. Because the characteristic slope (and λ) found for 0 and low NPA regressions implies a particular whorl diameter (d-b) for a given n_c (see Eq. 1), formation of the same n_c on larger embryos indicates that cotyledon whorls form more inset from the embryo edge in NPA-treated embryos than in control embryos.

Discussion

The intrinsic variability of cotyledon number (n_c) within conifer species (see Fig. 2 legend: std. dev. $s_c \approx 1.8$ cotyledons, with narrow confidence intervals) indicates a patterning process which is not genetically determined for a particular outcome (as in dicots), and provides a unique opportunity to study the control of spatial patterning during the process of development. Conifer cotyledon positioning involves more complex pattern formation than in monocots or dicots: the placement of 3 or more cotyledons on a 2D surface has many more potential options than the placement of 1 or 2 cotyledons, and the 3D geometry of the embryo is also a factor. A distinctive feature of conifer development is that cotyledons form in whorls, effectively reducing the dimensionality of the patterning, from placement on a 2D surface to placement in a quasi-1D ring (red, Fig. 1*e*). We refer to this radial aspect of cotyledon patterning as **P1**, or whorl positioning. In normal development, cotyledons are also spaced evenly in the circumferential dimension (**P2**) within this whorl (black spots, λ, Fig. 1*ef*).

Both λ and the radial inset of the whorl can be found from a linear regression of diameter vs. n_c (for CoN embryos), measured at the earliest appearance of cotyledons. From Eq. 1, the regression slope corresponds to λ (**P2** patterning) and the y-intercept corresponds to the radial inset (**P1** patterning). Comparison of our large Douglas fir and spruce samples with the earlier larch data (Harrison and von Aderkas 2004) indicates that inter-cotyledon spacing λ, on the order of 100-110 µm, is a conserved and reproducible feature of conifer development.

Embryo geometry at which cotyledon pattern established

Patterning on a disk has a theoretical slope/intercept ratio of 0.56 (for the first zero of the Bessel function, i.e. the first radial position at which a morphogen or growth catalyst would be zero; lower edge of the red band in Fig. 1*e*). The observed slope/intercept ratios for spruce and Douglas fir, however, are much lower than this (Fig. 4 legend); for a slope of around 35 µm/n_c (Fig. 4), the y-

intercept (237 µm for spruce, 284 µm for Douglas fir) is much larger than expected for patterning on a disk. This implies that the cotyledon pattern is not set on the disk-shaped top of the flattened embryo (Fig. 1*d*), but that it is set during flattening, between the dome-shaped (Fig. 1*c*) and the flat-topped (Fig. 1*d*) stages.

The Nagata et al. (2013) analysis for the flattening dome indicated that, to maintain a particular n_c, embryos would tend to grow in diameter as they flattened from a hemisphere to a disk. (Note: this analysis was for patterning of a single mechanism on the whole embryo surface, i.e. not constrained by **P1**.) As an estimate of embryo growth rate, we can compare initial measurements of diameter (when cotyledons first appear) to measurements approximately one week later (taken for verifying n_c). Fig. 7 shows the ratio of later/earlier diameter vs. n_c (same dataset as Fig. 3*a*). Roughly 75% of embryos show growth between the 1st and 2nd measurements. The analysis in Nagata et al. (2013, Fig. 5) indicates that pattern selection can change rapidly in the very first flattening stages (from γ = 1.0 to γ = 0.9; Fig. 1*e*), but then diameter needs to only increase gradually to maintain a particular n_c as the embryo flattens. (n_c is even robust to a slight decrease in diameter, particularly at low γ.) n_c is measured experimentally at the flattened-top stage (Fig. 1*d*); the Nagata et al. analysis indicates the measured n_c could have been patterned earlier at a much more domed stage, with minimal intervening diameter growth. For instance, a cotyledon whorl formed at the relatively domed γ = 0.75 would have the same n_c at the γ = 0.0 disk, as long as there was a 10% increase in diameter over this time. Pattern formation at γ = 0.9 would need a 20% diameter increase to maintain n_c at γ = 0.0. Fig. 7 indicates that embryo growth is largely within this 10-20% range, consistent with stable n_c over a large change in geometry (change in flatness).

Morphological effect of NPA is direct, not size dependent

NPA treatment induces a strong reduction of CoN morphology in favour of AnCR morphology (Table 1). The lack of a categorical diameter change in this morphological transition (Fig. 5) argues

against an indirect size effect altering **P2** to produce AnCR embryos (i.e. that diameter shrinkage would select annular pattern); but rather supports that NPA directly knocks out **P2** (circumferential) patterning. Retention of AnCR under NPA treatment indicates that cotyledon morphogenesis has 2 separable stages: a first stage, which does not require polar auxin transport, forming a ring of high growth (**P1** radial spatial pattern); and a second stage, requiring PAT, which determines the spacing and outgrowth of the cotyledons (**P2** circumferential spatial pattern) in that ring.

Robustness of inter-cotyledon spacing

Robustness of inter-cotyledon spacing λ was quantitatively measured with low-dose (0.02 to 0.06 μM) NPA treated CoN embryos: there was no difference in the slopes of the diameter–n_c regression lines for these NPA-treatment experiments vs. 0 NPA (for the spruce lines or for untreated fir (Fig. 4*b*) or larch (Harrison and von Aderkas 2004)).

CoN embryos forming at higher NPA concentrations (0.1 to 1.0 μM) also support that the inter-cotyledon spacing λ is not affected by NPA (Fig. 6; treatment data is consistent with the control slope). This indicates that the observed larger size of CoN embryos at these NPA levels (compared to control, at a given n_c) is associated with a larger radial inset of the whorl (y-intercept of the regression).

In general, CoN-Def and AnCR-Def embryos appear to have gaps in otherwise normal morphologies. AnCR-Def embryos show clefts in the ring and CoN-Def embryos show missing cotyledons, but radial ring formation appears intact, and circumferential inter-cotyledon spacing appears to retain the regular λ measured for CoN embryos. In terms of the Fig. 1*ef* schematic, for instance, a gap in a CoN-Def whorl would be loss of a black spot (or spots), but with the other spots staying in place, i.e. not shifting to fill the gap; see also Fig. 2*c*. Dumais and Harrison (2000, Fig. 3ac) observed a similar stability for λ spacing (but with a circumferential variation in initiation) in algal whorl morphogenesis.

Finally, while AnCR predominates above 0.08 μM NPA, we observed a decrease in 'rough ridge' AnCR embryos from intermediate NPA values (0.1 to 0.7 μM) to the highest concentration (1.0 μM). That is, embryo cups at 1.0 μM tended to have smoother rims, without circumferential inhomogeneities or patterning.

For a quasi-1D pattern such as **P2** (i.e. roughly sinusoidal along the circumferential coordinate within the whorl), an NPA effect could either be on the amplitude of the pattern (peak-to-trough concentration difference) or on the peak-to-peak spacing λ (the distance in μm between cotyledons). Together, the above evidence for a characteristic inter-cotyledon spacing (with or without NPA), the shift from CoN to AnCR with increasing NPA, and the decrease of any residual circumferential inhomogeneities ('roughness') at high NPA indicate that NPA affects the *amplitude* of the **P2** cotyledon pattern rather than the *spacing* (λ). This implies that without polar auxin transport, **P2** amplitude is 'flat' (no peak-trough difference; corresponding to no outgrowth of cotyledons). With PAT, **P2** amplitude can grow (be nonzero), corresponding to the outgrowth of cotyledons.

Mechanism for conifer cotyledon positioning

NPA treatment has a direct chemical effect on morphogenesis, showing that PAT is a necessary component in cotyledon outgrowth. While not ruling out a role for tissue mechanical properties in **P2** patterning, such an effect from blocking transport may more strongly suggest a chemical patterning mechanism, where transport provides the spatial dependence. Spatial patterning in PAT depends on a competition between passive ('down-the-gradient') transport (D) and active ('up-the-gradient') polar transport (T), with a wavelength dependent on the ratio D/T (Jönsson et al. 2006, Supp. Fig. 12). Insofar as cotyledon wavelength λ appears unaffected by the NPA decrease of T, this type of PAT patterning is not likely to be the mechanism for **P2** spacing. A Turing-type reaction-diffusion mechanism, with wavelength proportional to D/k (k representing local chemical reaction rates) would be unaffected by

NPA: reaction-diffusion would be consistent with the data for inter-cotyledon λ from CoN embryos and represents a potential mechanism for **P2** spacing. Whether the amplitude of a reaction-diffusion pattern grows or not can depend on precursor (reactant) concentrations: Harrison et al. (1981) were the first to apply this hierarchical idea to whorl formation (in algae), with a ring pattern producing a critical precursor for the circumferential pattern, thereby constraining organ formation in the radial dimension. Likewise, **P1** (the ring revealed by NPA treatment) could radially constrain a component necessary for the circumferential **P2** cotyledon pattern. Given the PAT-dependence of cotyledon outgrowth (**P2** amplitude growth; not the spacing λ), this component could involve PAT itself, with **P1** constraining PAT to the ring (and, if similar to the Furutani et al. 2014 study, NPA knockout of PAT 'drainage' could lead to excessive **P2** precursor, a condition which can cut off reaction-diffusion amplitude growth; Nagata et al. 2013). If instead PAT were non-localized (active more broadly over the embryo surface), the **P1** to **P2** control would be separate from PAT (and a more global NPA effect would also affect **P2** within the ring).

Recent molecular work in *Arabidopsis* shows ways in which complex morphogenetic phenomena can involve a combination of patterning mechanisms with different transport properties, such as the PAT-dependent vs. PAT-independent aspects of gynoecial development (Larsson et al. 2014); or the different directionality of different components of the PAT pathway in the shoot apex, where surface flow is associated with organ positioning and inward flow is associated with organ outgrowth (Furutani et al. 2014). The present work indicates that in conifers, similarly, complex morphogenesis may involve components with different transport properties. We have used a quantitative approach and the phenomena of polycotyledony and n_c variability to characterize the radial (**P1**) and circumferential (**P2**) aspects of cotyledon positioning in conifer embryogenesis. This indicates that polar auxin transport is not necessary for **P1** ring formation or for setting the **P2** inter-cotyledon spacing (wavelength λ), but that it is important for cotyledon outgrowth (**P2** amplitude) - consistent with Furutani et al.'s finding of separability of organ positioning and organ outgrowth. We hope that our results may provide insight

into whorl formation in general, for instance in floral morphogenesis, as well as guiding future experiments in conifers as molecular techniques become more powerful.

Acknowledgements

We thank Patrick von Aderkas and Lisheng Kong (University of Victoria) for somatic embryo cultures, discussions and technical advice; Jacques Dumais for helpful comments on the manuscript; Elena Polishchuck and Jessie Chen (University of British Columbia) for culture maintenance and technical advice; at BCIT, the Biotechnology Program for laboratory facilities and Keith Turner, Joan Shellard, Sarah McLeod and Bryan Andrews for technical advice; and BCIT and NSERC Canada for financial support (Discovery Grant to DMH; Undergraduate Student Research Assistantships to BB, CW, JK and MW).

References

Attree, S.M., and Fowke, L.C. 1993. Embryogeny of gymnosperms: advances in synthetic seed technology of conifers. Plant Cell Tissue Organ Cult. **35**: 1–35.

Bassel, G.W., Stamm, P., Mosca, G., Barbier de Reuille, P., Gibbs, D.J., Winter, R., Janka, A., Holdsworth, M.J., and Smith, R.S. 2014. Mechanical constraints imposed by 3D cellular geometery and arrangement modulate growth patterns in the *Arabidopsis* embryo. Proc. Nat. Acad. Sci. USA **111**: 8685 – 8690.

Bilsborough, G.D., Runions, A., Barkoulas, M., Jenkins, H.W., Hasson, A., Galinha, C., Laufs, P., Hay, A., Prusinkiewicz, P., and Tsiantis, M. 2011. Model for the regulation of *Arabidopsis thaliana* leaf margin development. Proc. Nat. Acad. Sci. USA **108**: 3424-3429.

Butts, D., and Buchholz, J.T. 1940. Cotyledon numbers in conifers. Trans. Illinois Acad. Sci. **33**: 58-62.

de Reuille, P.B., Bohn-Courseau, I., Ljung, K., Morin, H., Carraro, N., Godin, C., and Traas, J. 2006. Computer simulations reveal properties of the cell-cell signalling network at the shoot apex in *Arabidopsis.* Proc. Nat. Acad. Sci. USA **103**: 1627-1632.

Digiuni, S., Schellmann, S., Geier, F., Greese, B., Pesch, M., Wester, K., Dartan, B., Mach, V., Srinivas, B.P., Timmer, J., Fleck, C., and Hülskamp, M. 2008. A competitive complex formation mechanism underlies trichome patterning in *Arabidopsis* leaves. Mol. Sys. Biol.**4**: article 217.

Dumais, J., and Harrison, L.G. 2000. Whorl morphogenesis in the dasycladalean algae: the pattern formation viewpoint. Phil. Trans. R. Soc. Lond. **B355**: 281-305.

Friml, J. 2003. Auxin transport – shaping the plant. Curr. Opin. Plant Biol. **6**: 7-12.

Furutani, M., Nakano, Y., and Tasaka, M. 2014. MAB4-induced auxin sink generates local auxin gradients in *Arabidopsis* organ formation. Proc. Nat. Acad. Sci. USA **111**: 1198-1203.

Hakman, I., Hallberg, H., and Palovaraa, J. 2009. The polar auxin transport inhibitor NPA impairs embryo morphology and increases expression of an auxin efflux facilitator protein PIN during *Picea abies* somatic embryo development. Tree Physiol. **29**: 483-496.

Hamant, O., Heisler, M.G., Jönsson, H., Krupinksi, P., Uyttewaal, M., Bokov, P., Corson, F., Sahlin, P., Boudaoud, A., Meyerowitz, E.M., Couder, Y., and Traas, J. 2008. Developmental patterning by mechanical signals in *Arabidopsis*. Science **322**: 1650 – 1655.

Harrison, L.G., Snell, J., Verdi, R., Vogt, D.E., Zeiss, G.D., and Green, B.R. 1981. Hair morphogenesis in *Acetabularia mediterranea*: temperature-dependent spacing and models of morphogen waves. Protoplasma **106**: 211-221.

Harrison, L.G., and von Aderkas, P. 2004. Spatially quantitative control of the number of cotyledons in a clonal population of somatic embryos of hybrid larch *Larix* x *leptoeuropaea*. Ann. Bot. **93**: 423 – 434.

Holloway, D.M., and Harrison, L.G. 1999. Algal morphogenesis: modelling interspecific variation in *Micrasterias* with reaction-diffusion patterned catalysis of cell surface growth. Phil. Trans. R. Soc. Lond. ***B354***: 417 - 433.

Holloway, D.M., and Harrison, L.G. 2008. Pattern selection in plants: coupling chemical dynamics to surface growth in three dimensions. Ann. Bot. **101**: 361-374.

Jönsson, H., Heisler, M., Reddy, G.V., Agrawal, V., Gor, V., Shapiro, B.E., Mjolsness, E., and Meyerowitz, E.M. 2005. Modeling the organization of the WUSCHEL expression domain in the shoot apical meristem. Bioinformatics **21 [Suppl.]**: i232 – i240.

Jönsson, H., Heisler, M.G., Shapiro, B.E., Mjolsness, E., and Meyerowitz, E.M. 2006. An auxin-driven polarized transport model for phyllotaxis. Proc. Nat. Acad. Sci. USA **103**: 1633-1638.

Kroeger, J.H., Zerzour, R., and Geitmann, A. 2011. Regulator or driving force? The role of turgor pressure in oscillatory plant cell growth. PLoS ONE **6**: e18549.

Lacalli, T.C. 1981. Dissipative structures and morphogenetic pattern in unicellular algae. Phil. Trans. R. Soc. Lond. **B294**: 547 - 588.

Larsson, E., Sitbon, F., Ljung, K., and von Arnold, S. 2008. Inhibited polar auxin transport results in aberrant embryo development in Norway spruce. New Phytologist **177**: 356 – 366.

Larsson, E., Sundström, J.F., Sitbon, F., and von Arnold, S. 2012a. Expression of PaNAC01, a Picea abies CUP-SHAPED COTYLEDON orthologue, is regulated by polar auxin transport and associated with

differentiation of the shoot apical meristem and formation of separated cotyledons. Ann. Bot. **110**: 923-934.

Larsson, E., Sitbon, F., and von Arnold, S. 2012b. Differential regulation of Knotted1-like genes during establishment of the shoot apical meristem in Norway spruce (Picea abies). Plant Cell Rep. **31**: 1053-1060.

Larsson, E., Roberts, C.J., Claes, A.R., Franks, R.G., and Sundberg, E. 2014. Polar auxin transport is essential for medial versus lateral tissue specification and vascular-mediated valve outgrowth in *Arabidopsis* gynoecia. Plant Physiol. **166**: 1998-2012.

Laskowski, M., Grieneisen, V.A., Hofhuis, H., ten Hove, C.A., Hogeweg, P., Maree, A.F.M., and Scheres, B. 2008. Root system architecture from coupling cell shape to auxin transport. PLoS Biol. **6**: e307.

Martynov, L.A. 1975. A morphogenetic mechanism involving instability of initial form. J. Theor. Biol. **52**: 471 -480.

Meinhardt, H. 1984. Models of pattern formation and their application to plant development. In: *Positional Controls in Plant Development*, P.W. Barlow & D.J. Carr, (Eds.), Chap. 1. Cambridge University Press.

Mitchison, G.J. 1981. The polar transport of auxin and vein patterns in plants. Phil. Trans. R. Soc. Lond. **B 295**: 461-471.

Nagata, W., Zangeneh, H.R.Z., and Holloway, D.M. 2013. Reaction-diffusion patterns in plant tip morphogenesis: bifurcations on spherical caps. Bull. Math. Biol. **75**: 2346-2371.

Palovaraa, J., Hallberg, H., Stasolla, C., Luit, B., and Hakman, I. 2010a. Expression of a gymnosperm *PIN* homologous gene correlates with auxin immunolocalization pattern at cotyledon formation and

in demarcation of the procambium during *Picea abies* somatic embryo development and in seedling tissues. Tree Physiol. **30**: 479-489.

Palovaraa, J., Hallberg, H., Stasolla, C., and Hakman, I. 2010b. Comparative expression pattern analysis of *WUSCHEL-related homeobox 2* (*WOX2*) and *WOX8/9* in developing seeds and somatic embryos of the gymnosperm *Picea abies.* New Phytologist **188**: 122-135.

Rojas, E.R., Hotton, S., and Dumais, J. 2011. Chemically mediated mechanical expansion of the pollen tube cell wall. Biophysical J. **101**: 1844 – 1853.

Smith, R.S., Guyomarc'h, S., Mandel, T., Reinhardt, D., Kuhlemeier, C., Prusinkiewicz, P. 2006. A plausible model of phyllotaxis. Proc. Nat. Acad. Sci. USA **103**: 1301-1306.

Turing, A.M. 1952. The chemical basis of morphogenesis. Phil. Trans. R. Soc. Lond. **B237**: 37-72.

van Mourik, S., Kaufmann, K., van Dijk, A.D.J., Angenent, G.C., Merks, R.M.H., and Molenaar, J. 2012. Simulation of organ patterning on the floral meristem using a polar auxin transport model. PLoS ONE **7**: e28762.

von Aderkas, P. 2002. *In vitro* phenotypic variation in larch cotyledon number. Int. J. Plant Sci. **163**: 301-307.

Table 1: Cotyledon to cup-shaped ratios CoN : AnCR (*percentage CoN*), for different NPA concentrations

[NPA] (µM)	0	0.02	0.04	0.06	0.08	0.1	0.4	0.7	1.0
Spruce line									
SK	348 : 7 (*98%*)					21 : 182 (*10%*)	5 : 308 (*1.6%)*	4 : 269 *(1.4%)*	3 : 279 (*1.1%*)
2L13 (expt. 1)	25 : 6 (*81%*)	22 : 2 (*92%*)	21 : 2 (*91%*)	20 : 4 (*83%*)	8 : 19 (*30%*)				
2L13 (expt. 2)	3 : 41 (*6.8%*)	3 : 35 (*7.9%*)	1 : 26 (*3.7%*)	0 : 28 (*0%*)	0 : 27 (*0%*)				
2L13 (expt. 3)	6 : 34 (*15%*)	3 : 40 (*7.0%*)	1 : 36 (*2.7%*)	0 : 19 (*0%*)	0 : 17 (*0%*)				

Figure Captions

Fig. 1. Positioning conifer cotyledons on the surface of the embryo. (*a*, *b*) cotyledons form with a characteristic spacing, λ, within a whorl. Cotyledon numbers vary between individuals due to variation in diameter (scale bars are 250 μm in (*a*) and 200 μm in (*b*); these are older larch embryos, with substantial cotyledon outgrowth; adapted from Harrison and von Aderkas 2004, with permission). (*c*, *d*) cotyledon patterning occurs during a change in embryo geometry, from a hemispherical dome (*c*) to a flattened top (*d*). Red arrows show the first visible sign of cotyledon initials (larch embryos, adapted from Nagata et al. 2013, with permission). Line segment *d* represents the measured diameter (Eq. 1). (*e)* Representation of the embryo geometry and the factors involved in positioning the cotyledons. Polar coordinates for a circular embryo, with radial coordinate *r* and circumferential coordinate (longitude) ϕ. A point on the early-stage (hemispherical) dome would also have a latitude (θ) coordinate; as the embryo flattens, θ decreases and the geometry becomes more disk-like. The γ parameter specifies flatness, varying between γ = 1 (hemisphere) and γ = 0 (disk). (*f*) is a top-view of the geometry, with the *r*, ϕ coordinate system and parameters as above (adapted from Harrison and von Aderkas 2004, with permission). There are two aspects to positioning the cotyledons (black spots) on such a surface (see text): **P1** - constraining cotyledons to form in a whorl, at a certain radial distance from the embryo's tip or its outer edge (inset, *b*/2) of the morphogenetic tissue (red, *e*); and **P2 -** setting the inter-cotyledon spacing, λ, within the whorl (along the ϕ coordinate). λ/π is the slope and *b* is the y-intercept in Eq. 1. The diameter of the cotyledon whorl is (*d*-*b*).

Fig. 2. Classification of embryo morphologies: (*a*) CoN, normal cotyledon development (n_c = 9); (*b*) AnCR, cup-shaped embryo; (*c*) CoN-Def – in this example, 2 cotyledons form adjacent to one another, leaving a smooth gap of about 3 cotyledon-widths in the rest of the ring. Douglas fir, light photographs through the dissecting microscope, not to scale.

Fig. 3. Histograms of number of cotyledons (n_c) in somatic embryos (frequency is numbers of embryos). (*a*) Spruce (*Picea sitchensis*), SK line. Sample statistics: *N* = 326 embryos; mean, $\overline{n}_c$ = 5.8 (95% confidence interval CI [5.6, 6.0]); std. dev., s_c = 1.9 (95% CI [1.8, 2.1]). (*b*) Douglas fir (*Pseudotsuga menziesii*). Sample statistics: *N* = 127 embryos; $\overline{n}_c$ = 5.3 (95% CI [5.0, 5.6]); s_c = 1.8 (95% CI [1.6, 2.0]).

Fig. 4. Scatterplots of embryo diameter versus number of cotyledons, n_c. (*a*) spruce, (*b*) Douglas fir, same data as Fig. 3. Linear correlation is statistically significant for both species. The linear regression gives a very similar slope for both species (the regression shown does not include the two n_c 12 and 13 spruce embryos). Using Eq. 1, this indicates within-whorl, between-cotyledon (**P2**) spacing of λ = 110 μm for both species. The slope/intercept ratios for spruce (0.145, 95% CI [0.099, 0.21]; *a*) and Douglas fir (0.125, 95% CI [0.066, 0.22]; *b*) indicate that patterning occurs prior to the flattened-dome stage (Fig. 1*d*), see Discussion. (*c*, *d*) mean diameter with 95% CI for each n_c, for spruce (*c*) and Douglas fir (*d*).

Fig. 5. NPA induced reduction of CoN embryos does not depend on diameter change. (*a*, *b*) Histograms of diameters (in μm) for CoN (white bars with squares on top) and AnCR (dark grey bars with circles on top) embryos (2L13 spruce line). (Histograms overlaid, not stacked, i.e. white and grey bars both start at *y* = 0; black circles indicate top of a grey bar when hidden behind white.) Frequency is in embryo numbers. (*a*) 0 NPA control experiments; (*b*) 0.08 μM NPA treatment. Mean diameters are the same for CoN and AnCR embryos, for control and treatment. (*c*) Boxplots of embryo diameter (in μm), for concentrations from 0 to 0.08 μM NPA. No differences in diameter are observed between CoN and AnCR embryos. (*d*) Higher concentrations (SK spruce line) do begin to show reduced mean diameter in AnCR, compared to CoN; however, there is strong overlap between CoN and AnCR diameters at all NPA concentrations tested. Control (0 NPA) on left. For sample sizes, see Table 1.

Fig. 6. Cotyledon spacing (slope) at intermediate to high NPA concentration (0.1 to 1.0 μM) is consistent with spacing for untreated embryos. NPA-treated CoN embryos (red, green, yellow, black) overlaid on the n_c vs. diameter scatterplot of 0 NPA embryos (blue, same data as Fig. 4*a*; black line, 0

NPA regression). NPA-treated embryos tend to be larger than untreated controls. With the consistent slope, this indicates that cotyledons in NPA-treated embryos form more inset from the embryo edge than in controls.

Fig. 7. Boxplots of the ratio of later/earlier embryo diameter for each n_c (same dataset as Fig. 3*a*). The reference line at 1.0 indicates that about 75% of embryos are observed to grow in the week between measurements. Growth rates between 10% and 20% are typical (see reference line at 1.2), and would provide stable n_c over large changes in geometry (embryo flatness), according to the analysis in Nagata et al. (2013).

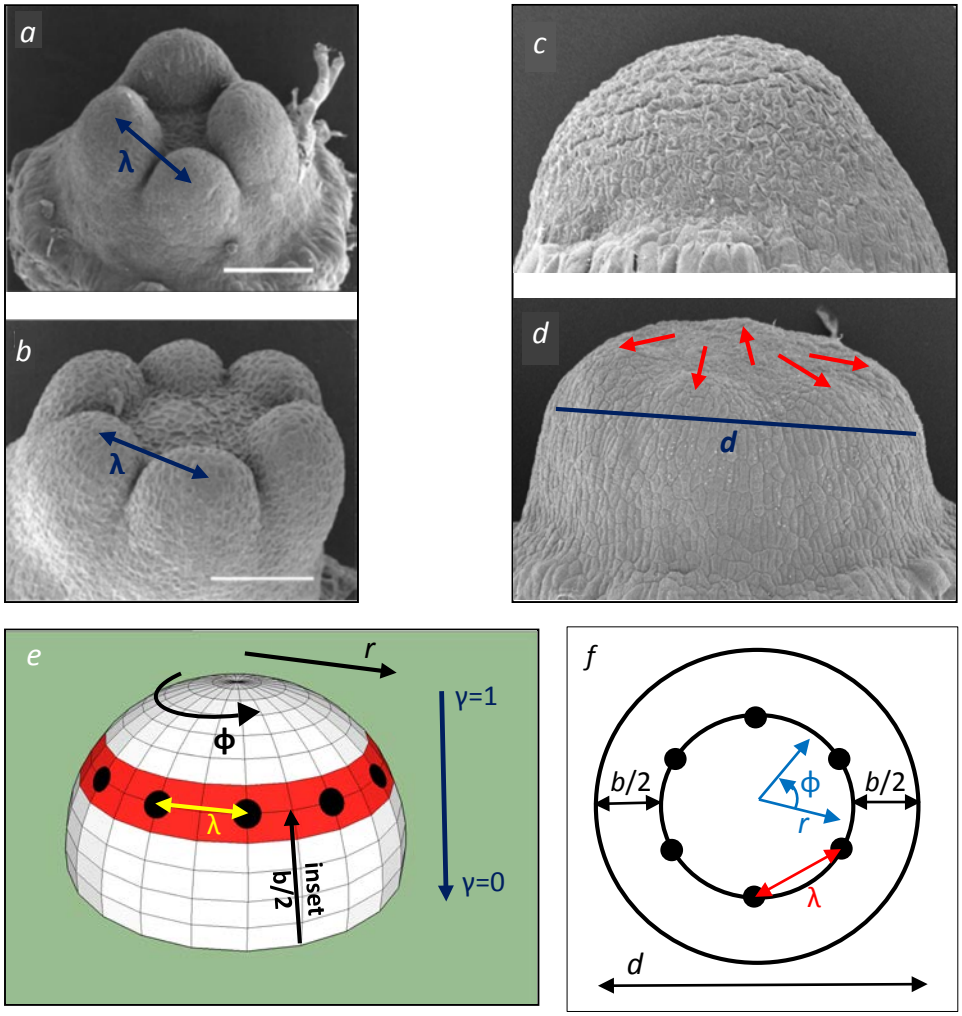

Figure 1

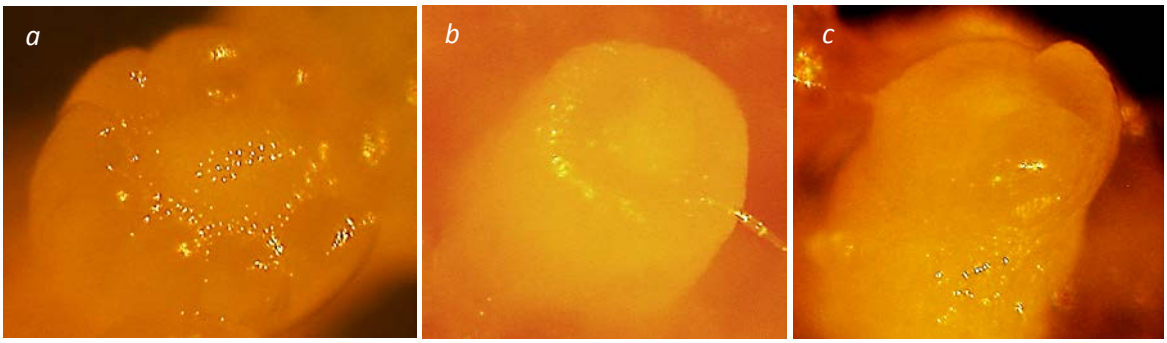

Figure 2

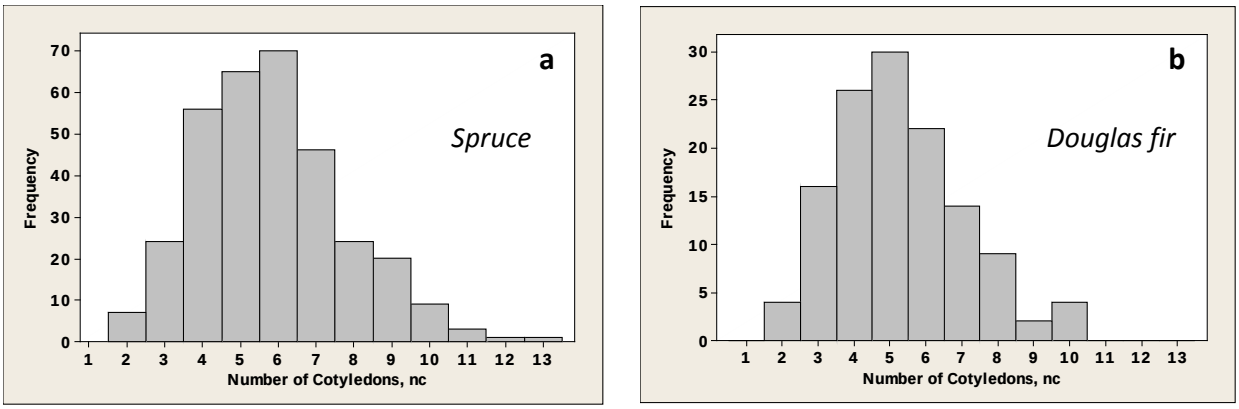
a
Spruce
Frequency
Number of Cotyledons, nc
b
Douglas fir
Frequency
Number of Cotyledons, nc

Figure 3

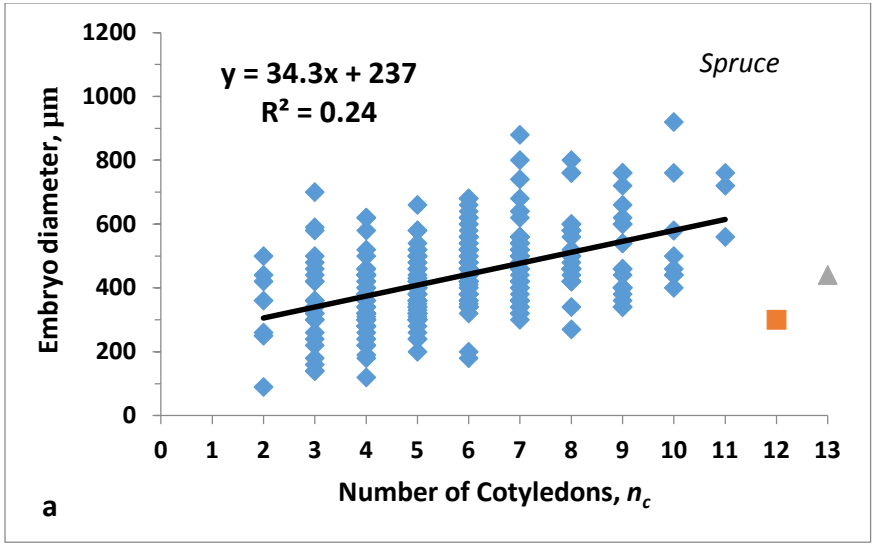
y = 34.3x + 237
R² = 0.24
Spruce
Embryo diameter, µm
Number of Cotyledons, n_c
a

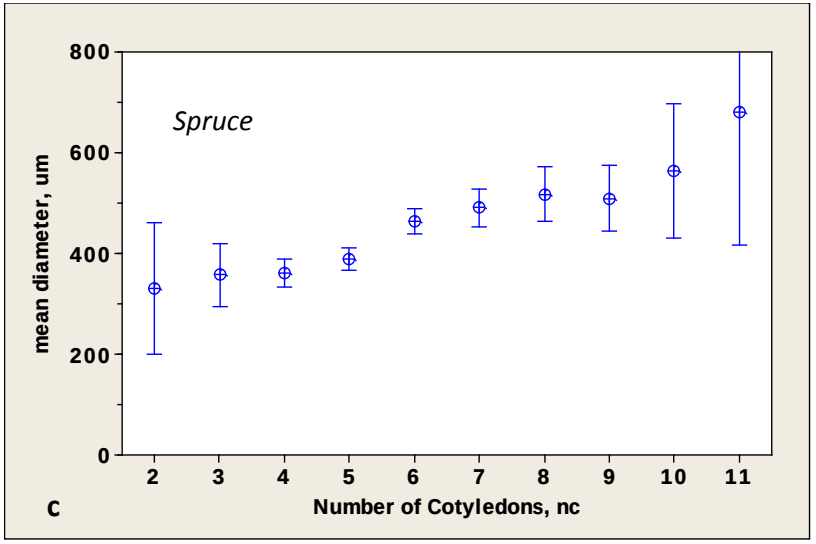
Spruce
mean diameter, um
Number of Cotyledons, nc
c

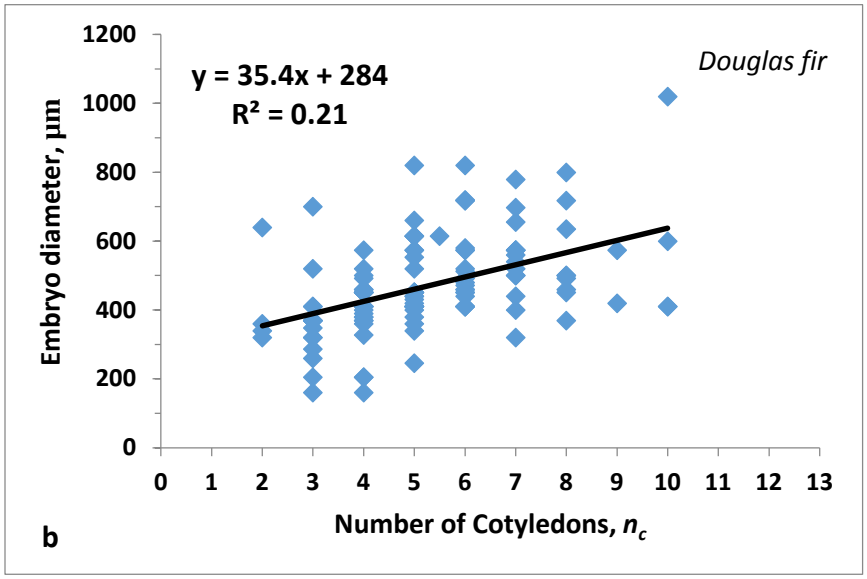
y = 35.4x + 284
R² = 0.21
Douglas fir
Embryo diameter, µm
Number of Cotyledons, n_c
b

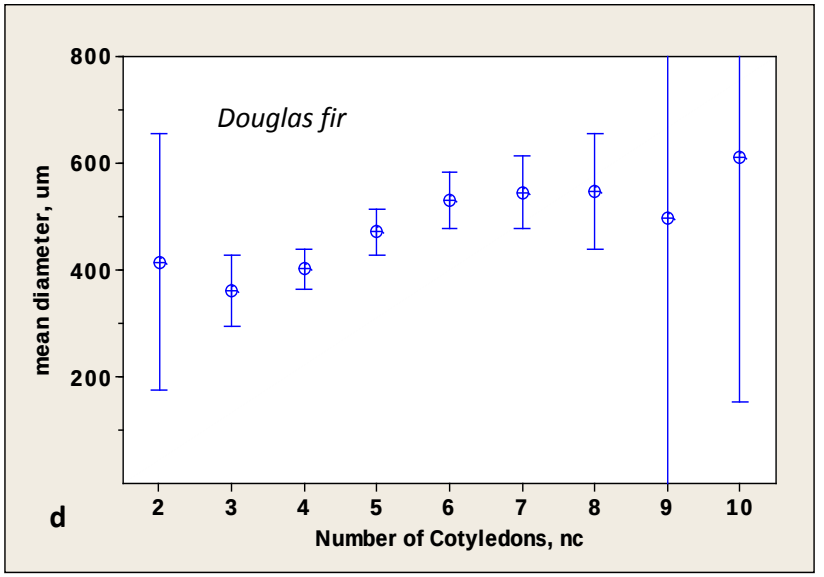
Douglas fir
mean diameter, um
Number of Cotyledons, nc
d

Figure 4

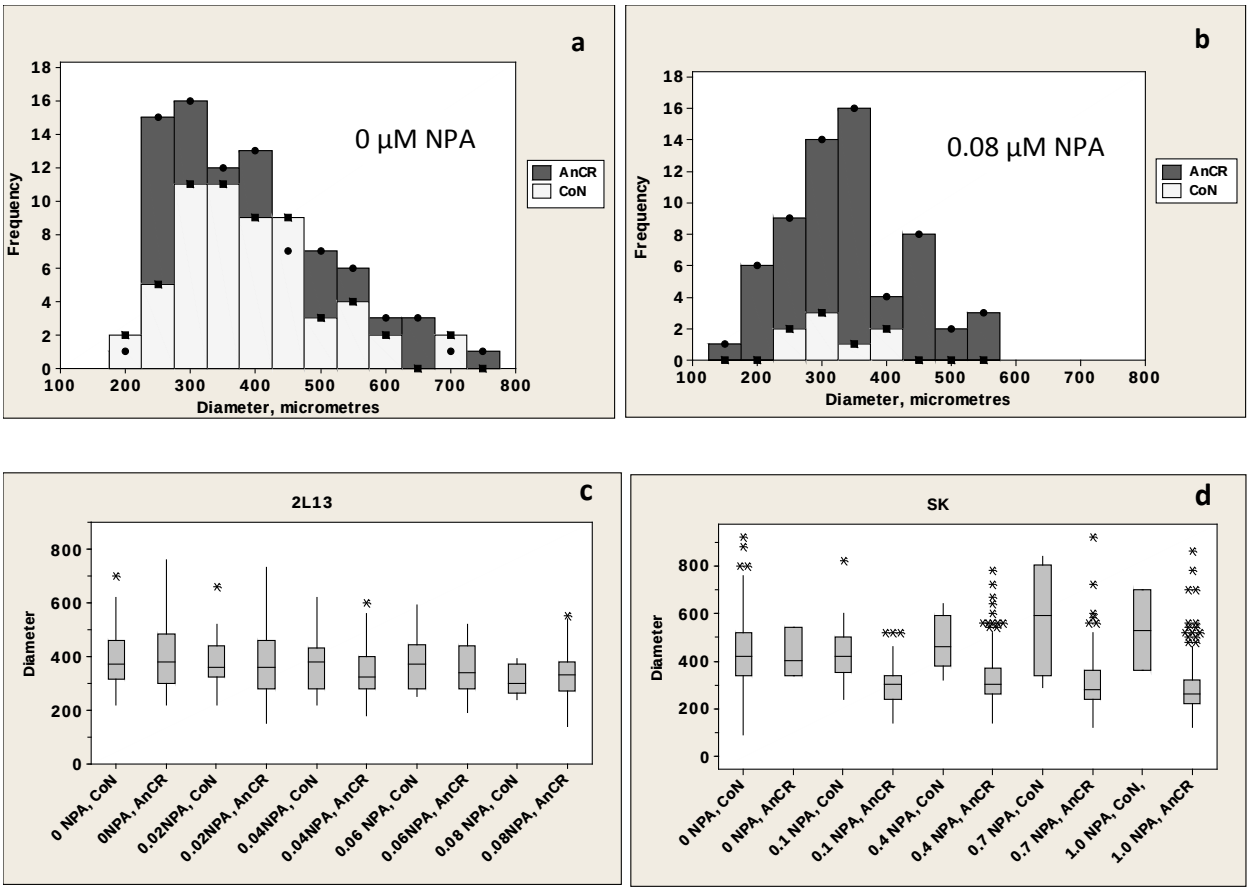
a
0 µM NPA
AnCR
CoN
Frequency
Diameter, micrometres
b
0.08 µM NPA
AnCR
CoN
Frequency
Diameter, micrometres
c
2L13
Diameter
0 NPA, CoN
0NPA, AnCR
0.02NPA, CoN
0.02NPA, AnCR
0.04NPA, CoN
0.04NPA, AnCR
0.06 NPA, CoN
0.06NPA, AnCR
0.08 NPA, CoN
0.08NPA, AnCR
d
SK
Diameter
0 NPA, CoN
0 NPA, AnCR
0.1 NPA, CoN
0.1 NPA, AnCR
0.4 NPA, CoN
0.4 NPA, AnCR
0.7 NPA, CoN
0.7 NPA, AnCR
1.0 NPA, CoN,
1.0 NPA, AnCR

Figure 5

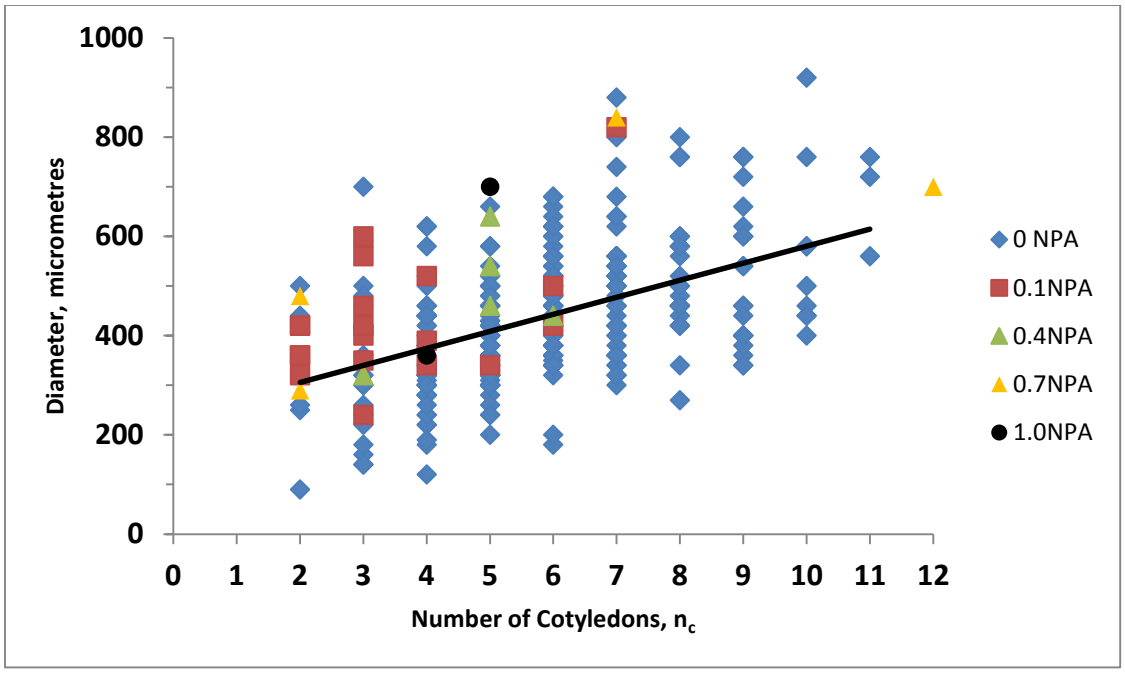
1000
800
600
400
200
0
Diameter, micrometres
0
1
2
3
4
5
6
7
8
9
10
11
12
Number of Cotyledons, n_c
0 NPA
0.1NPA
0.4NPA
0.7NPA
1.0NPA

Figure 6

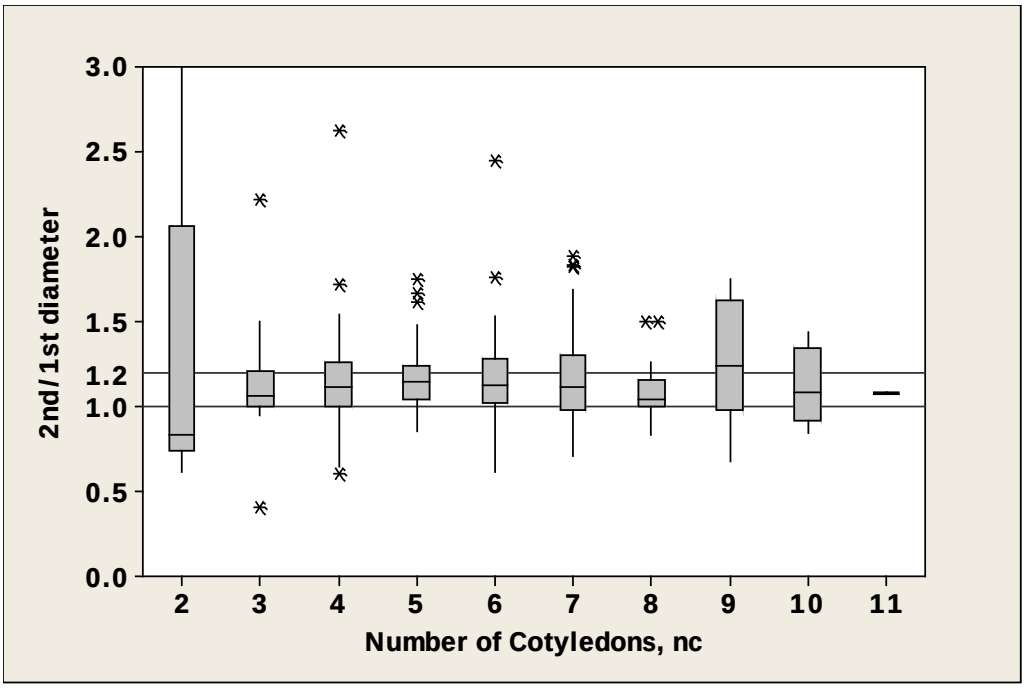
3.0
2.5
2.0
1.5
1.2
1.0
0.5
0.0
2nd/1st diameter
2
3
4
5
6
7
8
9
10
11
Number of Cotyledons, nc

Figure 7